Synthesis, Characterization, and Photochemistry of a Dinuclear Cyanide-Bridged Iron(II)−Platinum(IV) Mixed-Valence Compound and Its Implications for the Corresponding Iron(II)−Platinum(IV)−Iron(II) Complex

Brian W. Pfennig,* Jenny V. Lockard, and Jamie L. Cohen

Department of Chemistry, Vassar College, 124 Raymond Avenue, Poughkeepsie, New York 12604

David F. Watson, Douglas M. Ho, and Andrew B. Bocarsly

Department of Chemistry, Princeton University, Washington Road, Princeton, New Jersey 08544

Received December 17, 1998

The mixed-valence compound $[(NH_3)_5Pt^{IV}(\mu\text{-}NC)Fe^{II}(CN)_5]\cdot 6H_2O$ was synthesized by the substitution reaction of $[Pt^{IV}(NH_3)_5OSO_2CF_3](OSO_2CF_3)_3$ and $[Fe^{II}(CN)_6]^{4-}$ in aqueous solution and was characterized by UV/vis, IR, and resonance Raman spectroscopies, cyclic voltammetry, and single-crystal X-ray diffractometry. The monoclinic crystal (space group $P2_1/m$ (No. 11)) consists of a dinuclear, cyanide-bridged Fe(II)−Pt(IV) moiety with unit cell dimensions of $a = 9.3241(5)$ Å, $b = 14.0466(7)$ Å, $c = 9.6938(4)$ Å, $\beta = 111.467(2)°$, and $Z = 2$. There are also an average of six waters of hydration per unit cell. The *R*-factors for this structure are $R = 3.66\%$ and $R_w = 7.90\%$. The electronic spectrum reveals a broad intervalent (IT) charge-transfer absorption at approximately 420 nm ($\epsilon = 540\ M^{-1}\ cm^{-1}$). Both the ground-state spectroscopy and the electrochemistry of this compound are very similar to those of the corresponding trinuclear adduct $[(NC)_5Fe^{II}(\mu\text{-}CN)Pt^{IV}(NH_3)_4(\mu\text{-}NC)Fe^{II}(CN)_5]^{4-}$, which has been reported previously. Classical Marcus−Hush theory has been applied in the analysis of the IT band of the dinuclear compound in an effort to elucidate a fuller understanding of the photophysics of the trinuclear complex. The data suggest that this latter, centrosymmetric species can be treated theoretically as two back-to-back dinuclear donor−acceptor (D−A) compounds of the form D−A/A−D, where the Pt(IV) inversion center acts as the acceptor for both halves of the molecule. The photochemistry of the dinuclear complex was also investigated.

Introduction

Within the realm of inorganic photochemistry, the mixed-valence complex $[(NC)_5Fe^{II}(\mu\text{-}CN)Pt^{IV}(NH_3)_4(\mu\text{-}NC)Fe^{II}(CN)_5]^{4-}$ and its related congeners are fairly unique, both because of their centrosymmetric nature and because of their ability to undergo photoinduced, multielectron charge transfer following irradiation of their respective intervalent (IT) absorption bands.[1−4] For instance, irradiation of an aqueous solution of $[(NC)_5Fe^{II}(\mu\text{-}CN)Pt^{IV}(NH_3)_4(\mu\text{-}NC)Fe^{II}(CN)_5]^{4-}$ at 488 nm leads to the formation of $[Pt^{II}(NH_3)_4]^{2+}$ and 2 equiv of $[Fe^{III}(CN)_6]^{3-}$, a net two-electron process. Photoinduced multielectron-transfer processes are of interest from the standpoint of photocatalysis, solar energy conversion, and artificial photosynthesis, as well as from a theoretical point of view.[5] The photochemistry of this class of mixed-valence compounds has been successfully explained by using a three-parabola model (Figure 1c) in which the first electron is transferred photochemically by irradiation of the M(II) → Pt(IV) IT band to generate a Pt(III) intermediate. This intermediate is then capable of accepting a second electron thermally from the second cyanometalate.[2] The quantum efficiencies for photoproduct formation within this homologous family of trinuclear complexes have been explained in terms of the relative barriers to forward versus back electron transfer using this model and classical electron-transfer theory for class II (relatively localized) mixed-valence compounds.[4] Additionally, time-dependent resonance Raman theory has been used to estimate the relative nuclear distortions of the resonantly enhanced Raman modes associated with the photoinduced charge-transfer step.[6]

However, the degeneracy of the excited state associated with the centrosymmetric nature of these trinuclear compounds has raised some theoretical questions about the structure of this state, making it difficult to understand the detailed photophysics and the essential nature of the charge-transfer process.[7] The electronic states of inorganic charge-transfer complexes are typically approximated as harmonic oscillators, or as parabolas, in a plot of energy versus a one-dimensional nuclear coordinate. The trinuclear Fe(II)−Pt(IV)−Fe(II) complex requires at least a two-

* To whom correspondence should be addressed.

(1) Zhou, M.; Pfennig, B. W.; Steiger, J.; Van Engen, D.; Bocarsly, A. B. *Inorg. Chem.* **1990**, *29*, 2456.
(2) Pfennig, B. W.; Bocarsly, A. B. *J. Phys. Chem.* **1992**, *96*, 226.
(3) Pfennig, B. W.; Bocarsly, A. B. *Coord. Chem. Rev.* **1991**, *111*, 91.
(4) Wu, Y.; Cochran, C.; Bocarsly, A. B. *Inorg. Chim. Acta* **1994**, *226*, 251.
(5) (a) Zusman, L. D.; Beratan, D. N. *J. Chem. Phys.* **1996**, *105* (1), 165. (b) Balzani, V. *Pure Appl. Chem.* **1990**, *62*, 1099. (c) Collin, J. P.; Sauvage, J. P. *Coord. Chem. Rev.* **1989**, *93*, 245. (d) Heller, A. *Acc. Chem. Res.* **1981**, *14*, 154. (e) Scandola, F.; Argazzi, R.; Bignozzi, C. A.; Chiorboli, C.; Indelli, M. T.; Rampi, M. A. *Coord. Chem. Rev.* **1993**, *125*, 283.
(6) Pfennig, B. W.; Wu, Y.; Kumble, R.; Spiro, T. G.; Bocarsly, A. B. *J. Phys. Chem.* **1996**, *100*, 5745.
(7) Hennessy, M. H.; Wu, Y.; Bocarsly, A. B.; Soos, Z. G. *J. Phys. Chem. A* **1998**, *102*, 8312.

10.1021/ic981441a CCC: $18.00
Published on Web 05/15/1999

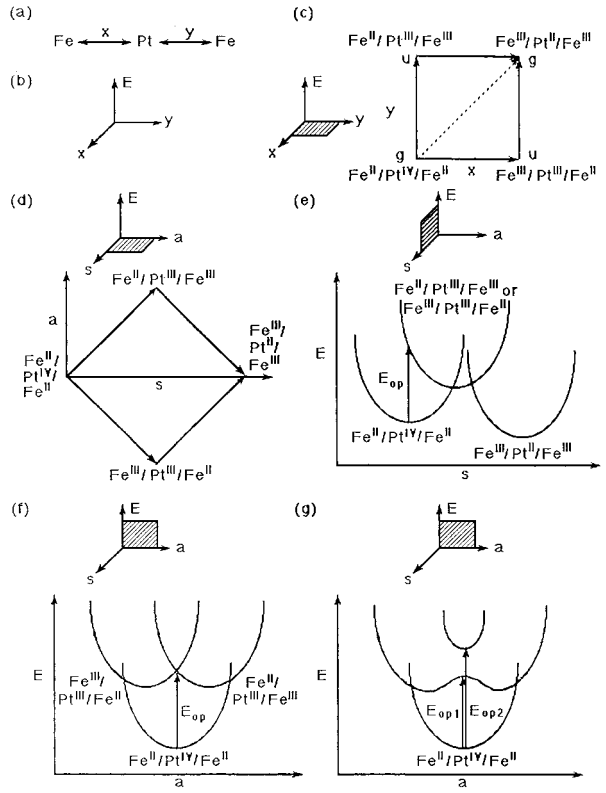

Figure 1. Theoretical analysis of the doubly degenerate IT absorption band in $[(NC)_5Fe^{II}(\mu\text{-}CN)Pt^{IV}(NH_3)_4(\mu\text{-}NC)Fe^{II}(CN)_5]^{4-}$ (abbreviated $Fe^{II}/Pt^{IV}/Fe^{II}$). (a) The initial photoinduced electron transfer causes a distortion along either the *x* nuclear coordinate to yield $Fe^{III}/Pt^{III}/Fe^{II}$ or the *y* nuclear coordinate to yield $Fe^{II}/Pt^{III}/Fe^{III}$. (b) The three-dimensional energy versus nuclear coordinate diagram, where all three axes are orthogonal. (c) The plane defined by the *x* and *y* nuclear coordinate axes, in which the locations of the four potential energy surface minima is shown. Solid arrows show the two allowed (g → u) initial electron-transfer steps and the two resulting thermal electron-transfer steps (u → g), while the dashed line shows the symmetry-forbidden (g → g), one-step, two-electron-transfer process. (d) Linear combinations of the *x* and *y* distortions have been taken to yield symmetric $(x + y)/2$, s, and antisymmetric $(x - y)/2$, a, nuclear coordinates. (e) Projection of the potential energy surfaces of the four states onto the plane defined by the symmetric coordinate and the energy axis. The one-electron intermediate is actually a pair of degenerate states. (f) Projection of the potential energy surfaces of the species onto the plane defined by the antisymmetric coordinate and energy axis. The $Fe^{III}/Pt^{II}/Fe^{III}$ products have been omitted to show the initial photoinduced one-electron process more clearly. (g) Representation of the possible electronic coupling between the degenerate $Fe^{III}-Pt^{III}-Fe^{II}$ and $Fe^{II}-Pt^{III}-Fe^{III}$ intermediates. Electronic coupling may give rise to two distinct IT energies.

dimensional nuclear coordinate. Therefore, a three-dimensional energy versus nuclear coordinate diagram is necessary to describe the net two-electron-transfer process. The Fe(II)−Pt(IV)−Fe(II) ground state has D_{4h} symmetry and is *gerade* with respect to the inversion center. The dissociated Fe(III), Pt(II), Fe(III) photoproducts are also *gerade* with respect to the inversion center, so a single two-electron-transfer step in which the molecule distorts symmetrically is a symmetry-forbidden process. If the electron transfer occurs in two steps, however, as the experimental evidence thus far suggests, then two intermediates are possible: Fe(III)−Pt(III)−Fe(II) and Fe(II)−Pt(III)−Fe(III), depending on which iron is involved in the initial electron-transfer step. Both of these intermediates are *ungerade* with respect to inversion, so the initial electron transfer is symmetry-allowed (g → u). We have simplified the problem by assigning the Fe(III)−Pt(III)−Fe(II) intermediate to be caused by a single, multimode distortion along the "*x*" nuclear coordinate, while the Fe(II)−Pt(III)−Fe(III) intermediate is caused by distortion along the "*y*" nuclear coordinate, as shown in Figure 1a. The three orthogonal axes of the energy versus nuclear coordinate diagram for the trinuclear complex are shown in Figure 1b. Once either of the two intermediates has formed, the second thermal electron transfer occurs to yield the dissociated photoproducts in another symmetry-allowed (u → g) process. Figure 1c shows the net two-electron-transfer process, where the labeled points depict the positions of the potential energy surface (parabolic cone) minima of each state in the plane defined by the *x* and *y* coordinates. Simply transforming coordinate systems from *x* and *y* into the symmetric $(x + y)/2$ and antisymmetric $(x - y)/2$ linear combinations of *x* and *y* yields the diagram illustrated in Figure 1d. This transformation nicely illustrates the net symmetric two-electron charge transfer as a linear combination of the requisite antisymmetric processes.

The presence of two intermediates may have significant implications in the energetics of the electron-transfer process of the trinuclear complex. Figure 1e represents the projection of the three-dimensional potential energy surfaces of the four electronic states onto the plane defined by the symmetric coordinate and the energy axis. This projection corresponds to the classic Marcus−Hush diagram of the charge-transfer process. Figure 1f represents the projection of the potential energy surfaces onto the plane defined by the antisymmetric coordinate and the energy axis. This projection shows that the Fe(II)−Pt(III)−Fe(III) and Fe(III)−Pt(III)−Fe(II) potential energy surfaces may overlap. If significant electronic coupling occurs, two nondegenerate states may result, giving rise to two closely spaced IT energies, as shown in Figure 1g. On the other hand, if little or no electronic coupling occurs between the two intermediates, then only one IT energy would exist. In this case, the trinuclear complex could be approximated as two back-to-back donor−acceptor (D−A) complexes, D−A/A−D, which happen to share the same acceptor. The shape and energy of the IT absorption band should depend on whether there is strong coupling between the two intermediate states. To determine which model is more accurate, we have synthesized and photophysically characterized the dinuclear compound, $[(NH_3)_5Pt^{IV}(\mu\text{-}NC)Fe^{II}(CN)_5]\cdot 6H_2O$. Due to its noncentrosymmetric nature, this dinuclear compound serves as an ideal model of the corresponding trinuclear complex, since only a single type of IT transition is possible, giving rise to only one intermediate.

Experimental Section

Materials and Apparatus. Trifluoromethanesulfonic (triflic) acid and $K_4Fe(CN)_6\cdot 3H_2O$ were purchased from Aldrich and were used without further purification. Bio-Gel P2 and P4 polyacrylamide gels were obtained from Bio-Rad. K_2PtCl_6 was synthesized by the addition of KCl to a concentrated aqueous solution of chloroplatinic acid. $[Pt(NH_3)_5(OSO_2CF_3)](OSO_2CF_3)_3$ was synthesized in two steps from K_2PtCl_6, according to literature procedures[8] and was boiled in chloroform prior to its use to remove $(CH_3CH_2)_2OH^+$. Infrared absorption spectra (KBr pellets) were collected as the average of four scans using a Nicolet Model 730 FTIR spectrometer with 4 cm^{-1} resolution. Electronic absorption spectra were collected in a 1 cm quartz cuvette at room temperature using a Hewlett-Packard HP8453 diode-array spectrophotometer with 2 nm resolution. Cyclic voltammograms were obtained in a 1 M $NaNO_3$ electrolyte solution by using a Princeton Applied Research (PAR) 173 potentiostat with a PAR 175 universal programmer, a Houston Instruments *XY* recorder, and a standard three-

(8) Curtis, N. J.; Lawrance, G. A.; Sargeson, A. M. *Inorg. Synth.* **1986**, *24*, 277.

electrode configuration (Pt/Pt/SCE). The quantum efficiency was determined at 488 nm by irradiating 1 mL samples (16 mM) with a Coherent Innova 70 argon ion laser (expanded beam) for 3−15 min and monitoring the disappearance of the IT absorption band at 488 nm (where none of the photoproducts have any significant absorption) and by monitoring the growth of the ferricyanide band at 303 nm. The incident light intensity (105 mW/cm^2) was measured with a calibrated Newport Research model 815 power meter.

Synthesis of $[(NH_3)_5Pt^{IV}(\mu\text{-}NC)Fe^{II}(CN)_5]\cdot 6H_2O$. To 70 mL of an aqueous solution of $[Pt(NH_3)_5(OSO_2CF_3)](OSO_2CF_3)_3$ (0.491 g, 0.560 mmol) was added with stirring 70 mL of aqueous $K_4Fe(CN)_6\cdot 3H_2O$ (0.237 g, 0.560 mmol). The solution changed from colorless to orange almost immediately and gradually deepened into a more reddish solution overnight. Upon standing, the resulting solution developed multiple red crystals which were deemed unsuitable for X-ray diffraction. The solution was further evaporated to a volume of ∼5 mL and then passed through a Bio-Gel P4 size exclusion column, yielding a dark red band (which was collected), followed by a minor yellow band. Upon slow evaporation of the former fraction, red platelets precipitated from the solution, and these were used for X-ray diffraction. The precipitate was filtered by vacuum and washed with two 10 mL portions of cold deionized water, followed by small portions of diethyl ether. The product was then stored at room temperature. Alternatively, noncrystalline samples of $[(NH_3)_5Pt^{IV}(\mu\text{-}NC)Fe^{II}(CN)_5]$ were synthesized more rapidly by combining equal amounts of 36 mM aqueous solutions of $K_4Fe(CN)_6\cdot 3H_2O$ and $[Pt(NH_3)_5(OSO_2CF_3)](OSO_2CF_3)_3$ with stirring to yield an orange, flocculent precipitate of the tight-ion pair $[Pt(NH_3)_5H_2O]^{4+}$, $[Fe(CN)_6]^{4-}$. The resulting mixture was heated at ∼95 °C for 10 min and then filtered by gravity to remove any remaining insoluble impurities. The pure product was obtained by passing the crude aqueous solution through a Bio-Gel P2 column and evaporating the first red-colored band to dryness.

Crystal Structure Determination. An orange plate, 0.08 mm × 0.21 mm × 0.22 mm in size, was sealed in a glass capillary and then transferred to a Nonius KappaCCD diffractometer equipped with Mo Kα radiation (λ = 0.710 73 Å) and a graphite monochromator. The diffraction method employed was ω scans; and the diffraction reflections limits for h, k, and l were −13 to +12, 0 to +13, and 0 to +19, respectively. Eight hundred frames of data were collected at 298(2) K with an oscillation range of 1°/frame and an exposure time of 60 s/frame.[9] Altogether, 19 329 reflections (θ_{max} = 30.08°) were indexed, integrated, and corrected for Lorentz and polarization effects using DENZO-SMN and SCALEPACK.[10] An ellipsoidal absorption correction was then applied using SHELXTL[11] to give 3587 unique reflections (R_{int} = 0.102) of which 3125 had $I > 2\sigma(I)$. The minimum and maximum transmission factors were 0.286 49 and 0.579 62, respectively. Post-refinement of the unit cell parameters gave a = 9.3241(5) Å, b = 14.0466(7) Å, c = 9.6938(4) Å, β = 111.467(2)°, and V = 1181.54(10) Å^3. The observed mean value for $|E^*E - 1|$ was 0.785. The structure was therefore initially solved in the chiral space group $P2(1)$. Tests for higher symmetry using PLATON-98[12] then revealed that the centrosymmetric monoclinic space group $P2(1)/m$ was preferred. Hence, all further computations were done in $P2(1)/m$ (No. 11). The structure was solved by direct methods and refined by full-matrix least squares on F^2 using SHELXTL.[11] All of the nonhydrogen atoms were refined with anisotropic displacement coefficients. The amine hydrogen atoms were assigned isotropic displacement coefficients U(H) = 1.5U(N), and their coordinates were allowed to ride on their respective nitrogens. Two waters [O(1W) and O(2W)] were located on sites of mirror symmetry and were included in the refinements with half-occupancies. Four additional water sites were found at general positions and the sum of their occupancy factors was restrained to 2.0 as follows: [O(3W), O(4W), O(5W), O(6W)] = [0.82(2), 0.32(2), 0.51(2), 0.35(2)]. Hydrogen atoms on all of the water molecules were not observed and were not included in the refinements. The weighting scheme employed was $w = 1/[\sigma^2(F_o^2) + (0.0345P)^2]$, where $P = (F_o^2 + 2F_c^2)/3$. The refinement converged to $R(F)$ = 0.0305, $R_w(F^2)$ = 0.0756, and S = 1.11 for 3125 reflections with $I > 2\sigma(I)$, and $R(F)$ = 0.0366, $R_w(F^2)$ = 0.0790, and S = 1.06 for 3586 unique reflections, 158 parameters, and 1 restraint.[13] One reflection (020) with a δ(F2)/σ value of 11.59 was considered aberrant and was suppressed. The maximum $\delta(F^2)/\sigma$ for the remaining 3586 unique reflections was 8.36 (for 135). The maximum $|\delta/\sigma|$ in the final cycle of least squares was 0.004, and the residual peaks on the final difference Fourier map ranged from −1.315 to +1.115 e Å^{-3}. Scattering factors were taken from the International Tables for Crystallography, Volume C.[14,15]

Resonance Raman Spectroscopy. Resonance Raman spectra were obtained in an aqueous solution containing 0.5 M K_2SO_4 (as an internal intensity standard) and 40 mM of the dinuclear compound. Due to the potential photochemical decomposition of the complex during the 25 min scans, Raman spectra were collected using a flow cell apparatus. Spectra were recorded in a 135° backscattering geometry[16] using a Spex 1877 triple monochromator equipped with a Princeton Instruments intensified diode array detection system. Laser excitation was obtained from either a Coherent Innova 100K3 Kr^+ ion or a Spectra Physics model 370 Ar^+ ion laser with incident irradiations of 30−40 mW (condensed beam). Both high (900−2250 cm^{-1}) and low (250−1100 cm^{-1}) frequency windows were recorded. The spectral windows were calibrated by obtaining the Raman spectrum of toluene or dimethyl-d_6 sulfoxide (DMSO-d_6) under identical optical alignment and using the known frequencies of these peaks in the correction. The raw data were corrected for the wavelength dependence of the monochromator entrance slit by multiplying the calibrated spectra by files of the square of the scattered wavelength vs Raman shift. Despite the fact that the compound undergoes photochemistry when irradiated into its IT absorption band, electronic spectra of the samples before and after the Raman experiments demonstrated that sample decomposition at this concentration and intensity of irradiation was negligible.

Results and Discussion

Synthesis and Characterization. Unlike the corresponding trinuclear ion, $[(NC)_5Fe^{II}(\mu\text{-}CN)Pt^{IV}(NH_3)_4(\mu\text{-}NC)Fe^{II}(CN)_5]^{4-}$, which forms by an inner-sphere electron-transfer process between $[Pt^{II}(NH_3)_4]^{2+}$ and two $[Fe^{III}(CN)_6]^{3-}$,[1] the dinuclear compound cannot be synthesized by a redox mechanism because of the absence of a suitable Pt(II) precursor and a second oxidizing equivalent. Therefore, a simple ligand substitution reaction was employed. It is well-known that the triflate ion is labile in aqueous solution and that coordination compounds containing this ligand as a leaving group will rapidly aquate.[17] Therefore, when aqueous solutions of $[Pt(NH_3)_5(OSO_2CF_3)](OSO_2CF_3)_3$ and $K_4Fe(CN)_6\cdot 3H_2O$ were combined in equimolar amounts, the lone pair electrons on one of the ferrocyanide ligands was anticipated to substitute for the labile ligand in the sixth coordination site of the platinum complex. The mixture rapidly developed a reddish-orange color with a broad electronic absorption developing at 421 nm. This peak was assigned as an Fe(II) → Pt(IV) intervalent (IT) absorption band, by analogy to the broad 424 nm absorption band in $[(NC)_5Fe^{II}(\mu\text{-}CN)Pt^{IV}$-

(9) *COLLECT Data Collection Software*; Nonius B. V. Rontgenweg: Delft, The Netherlands, 1998.
(10) Otwinowski, Z.; Minor, W. *Methods Enzymol.* **1997**, *276*, 307.
(11) Sheldrick, G. M. *SHELXTL*, Version 5; Siemens Analytical X-ray Instruments: Madison, WI, 1996.
(12) Spek, A. L. *Acta Crystallogr.* **1990**, *A46*, C34.
(13) $R(F) = R_1 = \sum(||F_o| - |F_c||)/\Sigma|F_o|$; $R_w(F^2) = R_{w2} = [\sum(w(F_o^2 - F_c^2)^2/\sum(w(F_o^2)^2]^{0.5}$; and S = goodness of fit on $F_2 = [\sum(w(F_o^2 - F_c^2)^2)/(n - p)]^{0.5}$, where n is the number of reflections and p is the number of parameters refined.
(14) Maslen, E. N.; Fox, A. G.; O'Keefe, M. A. *International Tables for Crystallography: Mathematical, Physical, and Chemical Tables*, Vol. C; Kluwer: Dordrecht, The Netherlands, 1992; pp 476−516.
(15) Creagh, D. C.; McAnley, W. J. *International Tables for Crystallography: Mathematical, Physical, and Chemical Tables*, Vol. C; Kluwer: Dordrecht, The Netherlands, 1992; pp 206−222.
(16) Spiro, T. G.; Czernuszewicz, R. S. in *Physical Methods in Bioinorganic Chemistry*; Que, L., Ed.; University Science Books: Mill Valley, CA, 1991.
(17) Dixon, N. E.; Lawrance, G. A.; Lay, P. A.; Sargeson, A. M. *Inorg. Chem.* **1983**, *22*, 846.

$(NH_3)_4(\mu\text{-NC})Fe^{II}(CN)_5]^{4-}$.[1] Infrared analysis of the red solid which resulted after purification yielded a spectrum which contained both bridging and terminal cyanide stretching absorptions (2119 and 2054 cm^{-1}, respectively). The IR spectrum also confirmed the oxidation states of the two metals as Fe(II) and Pt(IV), indicating that no redox process had occurred during the reaction. Platinum(IV) ammine compounds are characterized by NH stretches between 3050 and 3150 cm^{-1}, symmetric HNH bending modes at 1370 cm^{-1}, and rocking NH_3 vibrations at 950 cm^{-1} (compared to 3150−3250, 1325, and 842 cm^{-1} for platinum(II) ammines). The compound of interest exhibited these vibrations at 3000−3200, 1399, and 989 cm^{-1}, respectively. Ferrocyanide has a CN stretch at 2044 cm^{-1} and an Fe−C stretch at 585 cm^{-1} (compared to 2118 and 511 cm^{-1}, respectively, for ferricyanide).[18] The dinuclear compound possessed vibrations at 2054 and 585 cm^{-1}, corresponding to the terminal cyanide ligands. Bridging cyanide stretches are well-documented to occur from 50 to 90 cm^{-1} higher in energy than terminal cyanide stretches while the M−C stretches of bridged cyanide complexes are shifted to lower energies.[1,4,19] These absorptions occur in $[(NH_3)_5Pt^{IV}(\mu\text{-NC})Fe^{II}(CN)_5]$ at 2119 and 523 cm^{-1}, respectively.

Cyclic voltammetry of the compound in 1 M $NaNO_3$ over the scan rate range of 10−500 mV/s revealed a single, quasi-reversible peak with $E_{1/2} = 0.54$ V vs SCE. This redox wave has been assigned to the Fe(III)/Fe(II) couple, compared with an $E_R^\circ = 0.19$ V vs SCE observed for ferricyanide.[20] This positive shift has been observed for other bridged metallocyanide complexes and is a consequence of the removal of electron density from the Fe(II) center by formation of a coordinate covalent bond between the cyanide nitrogen and the Pt(IV) species.[1,2,4,19g] In fact, $E_{1/2} = 0.55$ V vs SCE for the iron moieties in $[(NC)_5Fe^{II}(\mu\text{-CN})Pt^{IV}(NH_3)_4(\mu\text{-NC})Fe^{II}(CN)_5]^{4-}$, which has similarly coordinated iron centers.[1] No redox wave for the platinum center within either of these compounds was observed. This is probably due to the slow charge-transfer kinetics of the process. Upon applying a 0 V vs SCE potential to the electrochemical cell, no significant current response was observed; however, if 1 V vs SCE was applied, an anodic current was observed. These findings indicate that the IR assignment of the iron oxidation state as 2+ is correct. Furthermore, single-crystal X-ray diffraction conclusively demonstrated the presence of a cyanide bridge between the two metals.

Resonance Raman Spectroscopy. The Raman spectrum of the dinuclear compound irradiated at 457.9 nm (on the red side of the IT band) exhibits the resonantly enhanced vibrational modes listed in Table 1. These modes have been tentatively assigned by analogy with those in the chemical literature for the trinuclear compound.[6] The two compounds have virtually identical resonance Raman spectra in terms of both the energies of the normal modes and their relative intensities, indicating that a model in which Fe(II)−Pt(IV)−Fe(II) can be considered as comprised of two noninteracting Fe(II)−Pt(IV) subunits sharing a common Pt(IV) atom can be postulated. A similar experiment using an off-resonance wavelength (676.4 nm) which does not lie in the IT absorption window revealed no observable resonantly enhanced Raman peaks for the dinuclear species. This indicates that the Raman peaks reported at 457.9 nm irradiation indeed correspond to distortions which relate to the IT excited state of the molecule. A detailed analysis of the excited-state distortion based on the resonance enhancement excitation profile for this molecule is currently under study and will be reported in the future.

Table 1. Resonance Raman Data for $[(NH_3)_5Pt^{IV}(\mu\text{-NC})Fe^{II}(CN)_5]$ and $[(NC)_5Fe^{II}(\mu\text{-CN})Pt^{IV}(NH_3)_4(\mu\text{-NC})Fe^{II}(CN)_5]^{4-}$, along with Their Tentative Peak Assignments

tentative peak assignm	dinuclear compd (cm^{-1})	trinuclear compd (cm^{-1})[6]
$\delta(H_3N-Pt-NH_3)$	297	299
$\nu(Pt-NC)$	368	366
$\delta(Fe-CN)$	426	422
$\nu(Pt-NH_3)_{out}$	475	472
$\nu(Pt-NH_3)_{in}$	508	506
$\nu(Fe-C)_{br}$	570	566
$\nu(Fe-C)_{rad}$	588	587
$\nu(Fe-C)_{ax}$	627	623
$\nu(CN)_{term}$	2082	2081
$\nu(CN)_{br}$	2126	2125

Crystal Structure. A summary of the crystallographic data for $[(NH_3)_5Pt^{IV}(\mu\text{-NC})Fe^{II}(CN)_5]\cdot 6H_2O$ appears in Table 2. The ellipsoids plot of the dinuclear compound (excluding the waters of hydration) is shown in Figure 2, and extended plots of the crystal structure along the *a*, *b*, and *c* axes are shown in Figures S1−S3 in the Supporting Information. Atomic coordinates ($\times 10^4$) and equivalent isotropic displacement parameters ($Å^2 \times 10^3$) are listed in Table S2 in the Supporting Information. Representative bond lengths and angles for the compound are listed in Table 3. The structure consists of a ferrocyanide moiety which is bridged via a single cyanide ligand to a pentaammineplatinum(IV) center. The local coordination around the iron center is octahedral with the coordination geometry of the platinum center having a tetragonally distorted *z*-in perturbation. Both the $Pt-N_{br}$ and $Pt-N_{ax}$ bond lengths are shorter than the average $Pt-N_{rad}$ bonds, as shown in Table 3. The X-ray structure also shows that the Fe and Pt radial ligands are in a *gauche* conformation such that the d_{xy} orbital on the Fe center is parallel to the $d_{x^2-y^2}$ orbital on Pt, providing the correct arrangement for maximum overlap of these orbitals. This result was also reported for the corresponding trinuclear Fe(II)−Pt(IV)−Fe(II) species[1] and is critical to the IT charge-transfer process. An examination of the extended crystalline structure reveals that the Fe and Pt moieties are stacked such that they align head-to-tail in the crystal in an alternating pattern. This crystal packing is reminiscent of ionic compounds and is probably due to the residual negative and positive partial charges on each half of the molecule. Two of the six waters of hydration lie between the stacks, while the other four partially occupy sites in the channels formed between stacks.

UV/vis Spectroscopy and Classical ET Analysis of the IT Band. The UV/vis spectrum of $[(NH_3)_5Pt^{IV}(\mu\text{-NC})Fe^{II}(CN)_5]$ exhibits two broad absorptions at 317 and 421 nm, with molar absorptivities of 400 and 540 M^{-1} cm^{-1}, respectively. The relative shapes and energies of these peaks are nearly identical to those of the trinuclear Fe(II)−Pt(IV)−Fe(II) adduct, with the exception of their intensities. A comparison of the physical properties of these two compounds is shown in Table 4. By analogy to the trinuclear compound, the absorption at 421 nm has been assigned as an intervalent transition from Fe(II) →

(18) Nakamoto, K. *Infrared and Raman Spectra of Inorganic and Coordination Compounds*, 4th ed.; John Wiley & Sons: New York, 1986.
(19) (a) Bignozzi, C. A.; Argazzi, R.; Schoonover, J. R.; Gordon, K. C.; Dyer, R. B.; Scandola, F. *Inorg. Chem.* **1992**, *31*, 5260. (b) Chatterjee, D.; Bajaj, H. C.; Das, A. *Inorg. Chem.* **1993**, *32*, 4049. (c) Lei, Y.; Buranda, T.; Endicott, J. F. *J. Am. Chem. Soc.* **1990**, *112*, 8820. (d) Doorn, S. K.; Dyer, R. B.; Stoutland, P. O.; Woodruff, W. H. *J. Am. Chem. Soc.* **1993**, *115*, 6398. (e) Vogler, A.; Kunkely, H. *Inorg. Chim. Acta* **1988**, *150*, 1. (f) Forlano, P.; Baraldo, L. M.; Olabe, J. A.; Della Védova, C. O. *Inorg. Chim. Acta* **1994**, *223*, 37. (g) Pfennig, B. W.; Goertz, J. K.; Wolff, D. W.; Cohen, J. L. *Inorg. Chem.* **1998**, *37*, 2608.
(20) Curtis, J. F.; Meyer, T. J. *Inorg. Chem.* **1982**, *21*, 1562.

Table 2. Summary of Crystallographic Data for $[(NH_3)_5Pt^{IV}(\mu\text{-NC})Fe^{II}(CN)_5]\cdot 6H_2O$

empirical formula	$C_6H_{15}FeN_{11}Pt\cdot 6H_2O$	*V*	1181.54 (10) Å^3
fw	600.33 g/mol	*Z*	2
space group	*P*2(1)/*m* (No. 11)	temp	25(2) °C
unit cell dimens		radiation	Mo Kα radiation (λ = 0.710 73 Å)
a	9.3241 (5) Å	density (calcd)	1.687 g/cm^3
b	14.0466 (7) Å	abs coeff	65.65 cm^{-1}
c	9.6938 (4) Å	*R*, R_w^2 (all data)[a]	0.0366, 0.0790
β	111.467 (2)°		

[a] $R(F) = R_1 = \sum(||F_o| - |F_c||)/\sum|F_o|$ and $R_w(F^2) = R_{w2} = [\sum w(F_o^2 - F_c^2)^2/\sum(w(F_o^2))^2]^{0.5}$.

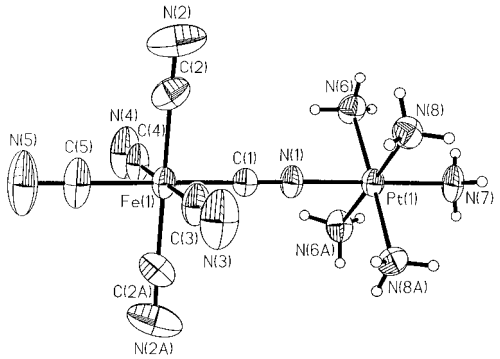

Figure 2. ORTEP diagram for the single-crystal X-ray study of $[(NH_3)_5Pt^{IV}(\mu\text{-NC})Fe^{II}(CN)_5]\cdot 6H_2O$ using a Nonius KappaCCD diffractometer. The six waters of hydration have been omitted for greater clarity.

Table 3. Representative Bond Distances (Å) and Bond Angles (deg) for the $[(NH_3)_5Pt^{IV}(\mu\text{-NC})Fe^{II}(CN)_5]\cdot 6H_2O$

Fe(1)−C(1)	1.876 (5)	C(2)−N(2)	1.145 (8)
Fe(1)−C(4)	1.901 (5)	C(3)−N(3)	1.153 (7)
Fe(1)−C(3)	1.903 (6)	C(4)−N(4)	1.150 (7)
Fe(1)−C(5)	1.906 (6)	C(5)−N(5)	1.149 (9)
Fe(1)−C(2)	1.910 (6)	Pt(1)−N(7)	2.023 (4)
C(1)−N(1)	1.135 (7)	Pt(1)−N(8)	2.040 (3)
N(1)−Pt(1)	1.987 (4)	Pt(1)−N(6)	2.052 (3)
C(1)−Fe(1)−C(4)	88.8 (2)	N(3)−C(3)−Fe(1)	178.1 (5)
C(1)−Fe(1)−C(3)	89.8 (2)	N(4)−C(4)−Fe(1)	177.7 (5)
C(4)−Fe(1)−C(3)	178.6 (2)	N(5)−C(5)−Fe(1)	179.0 (6)
C(1)−Fe(1)−C(5)	179.7 (2)	N(1)−Pt(1)−N(7)	178.4 (2)
C(4)−Fe(1)−C(5)	90.9 (2)	N(1)−Pt(1)−N(8)	88.98 (14)
C(3)−Fe(1)−C(5)	90.5 (2)	N(7)−Pt(1)−N(8)	89.9 (2)
C(1)−Fe(1)−C(2)	90.2 (2)	N(8)−Pt(1)−N(8A)	88.4 (2)
C(4)−Fe(1)−C(2)	90.42 (13)	N(1)−Pt(1)−N(6)	89.67 (14)
C(3)−Fe(1)−C(2)	89.58 (13)	N(7)−Pt(1)−N(6)	91.50 (14)
C(5)−Fe(1)−C(2)	89.8 (2)	N(6)−Pt(1)−N(8A)	178.43 (13)
N(1)−C(1)−Fe(1)	178.1 (5)	N(8)−Pt(1)−N(6)	92.4 (2)
C(1)−N(1)−Pt(1)	175.0 (5)	N(6)−Pt(1)−N(6A)	86.8 (2)
N(2)−C(2)−Fe(1)	177.9 (6)		

Pt(IV). Neither $[Fe(CN)_6]^{4-}$ nor $[Pt(NH_3)_6]^{4+}$ shows any electronic absorptions at this energy. The higher-lying peak at 317 nm, on the other hand, has previously been attributed to a combination of charge-transfer peaks due to the separate iron and platinum coordination complexes. The 1:1 stoichiometry of the compound in aqueous solution was confirmed using Job's method of continuous variations[21] by monitoring the IT absorption band intensity as a function of the iron:platinum ratio. From the sharply triangular shape of the Job plot, it was determined that the reaction between the two coordination complexes had gone essentially to completion to form the dinuclear adduct.

Classical Marcus−Hush theory was used to model the IT absorption band. Under the high-temperature classical limit, equations 1−5 can be employed for Robin and Day Class II mixed-valence compounds[22] in order to obtain kinetic information about the electron transfer using thermodynamic data.[23] In

Table 4. Summary of the Observed and Calculated Marcus−Hush Parameters for $[(NH_3)_5Pt^{IV}(\mu\text{-NC})Fe^{II}(CN)_5]$ and $[(NC)_5Fe^{II}(\mu\text{-CN})Pt^{IV}(NH_3)_4(\mu\text{-NC})Fe^{II}(CN)_5]^{4-}$ in Aqueous Solution

Marcus−Hush param	dinuclear compd	trinuclear complex
E_{op} (nm)	421	424
$\bar{\nu}_{max}$ (cm^{-1})	23,750	23,590
ϵ_{max} (M^{-1} cm^{-1})	540	2365
$\Delta\bar{\nu}_{1/2}$(cm^{-1})	7820	7170
$E°$ for the bridged Fe (V vs SCE)	0.54	0.55
$\Delta G°$ (kcal/mol)	25.4	25.6
χ (kcal/mol)	42.5	41.8
$\Delta G*$ (kcal/mol)	27.1	27.2
k_{et} at 298 K (s^{-1})	8.8×10^7	8.5×10^7
r (Å)	5.00	4.99
H_{ab} (cm^{-1})	1300	1840
α (unitless)	0.05	0.08

[a] Definitions of the abbreviations can be found in the text.

$$E_{op} = \chi + \Delta G° \quad (1)$$

$$\Delta G* = E_{op}/4\chi \quad (2)$$

$$k_{et} = A \exp\left\{\frac{-\Delta G*}{RT}\right\} \quad (3)$$

$$H_{ab} = 0.0205\left\{\frac{\epsilon_{max}\Delta\bar{\nu}_{1/2}}{\bar{\nu}_{max} g}\right\}^{1/2} \frac{\bar{\nu}_{max}}{(r/\text{Å})} \quad (4)$$

$$\alpha = [H_{ab}^2/\bar{\nu}_{max}^2]^{1/2} \quad (5)$$

these equations, E_{op} is the optical IT transition energy determined from the UV/vis, χ is the reorganization energy associated with the nuclear distortion and solvent reorientation, $\Delta G°$ is the ground-state redox potential difference between the donor and acceptor sites (obtainable from the electrochemistry), $\Delta G*$ is the thermal activation energy for the electron transfer, k_{et} is the corresponding electron-transfer rate constant, *A* is the Arrhenius preactivation constant (usually taken as $\sim 5 \times 10^{12}$ s^{-1} for electron-transfer reactions), H_{ab} (cm^{-1}) is a measure of the electronic coupling between the donor and acceptor, ϵ_{max} is the molar absorptivity of the IT band at its maximum value, $\Delta\bar{\nu}_{1/2}$ is the IT absorption bandwidth at half its maximum height (cm^{-1}), $\Delta\bar{\nu}_{max}$ is the energy of the IT absorption maximum in wavenumber units, *g* is the degeneracy, *r* is the distance (Å) between the donor and acceptor (which in this case is estimated

(21) Vosburgh, W. C.; Cooper, G. R. *J. Am. Chem. Soc.* **1941**, *63*, 437.

(22) Robin, M. B.; Day, P. *Adv. Inorg. Chem. Radiochem.* **1967**, *10*, 247.

(23) (a) Marcus, R. A. *J. Chem. Phys.* **1956**, *24*, 966. (b) Marcus, R. A. *J. Chem. Phys.* **1965**, *43*, 679. (c) Marcus, R. A.; Sutin, N. *Inorg. Chem.* **1975**, *14*, 213. (d) Hush, N. S. *Trans. Faraday Soc.* **1956**, *57*, 557. (e) Hush, N. S. *Electrochim. Acta* **1968**, *13*, 1005. (f) Hush, N. S. *Chem. Phys.* **1975**, *10*, 361. (g) Hush, N. S. *Prog. Inorg. Chem.* **1967**, *8*, 357. (h) Hush, N. S. *Prog. Inorg. Chem.* **1967**, *8*, 391.

from the Fe−Pt distance in the X-ray crystal structure),[24] and α is the delocalization parameter.

Using these equations, the observed and calculated Marcus−Hush parameters for both $[(NH_3)_5Pt^{IV}(\mu\text{-NC})Fe^{II}(CN)_5]$ and $[(NC)_5Fe^{II}(\mu\text{-CN})Pt^{IV}(NH_3)_4(\mu\text{-NC})Fe^{II}(CN)_5]^{4-}$ are listed in Table 4. With the exception of the molar absorptivity, the remainder of the parameters in Table 4 are remarkably similar for the two different compounds. We interpret these results to mean that the trinuclear Fe(II)−Pt(IV)−Fe(II) species can be treated theoretically as being composed of two Fe(II)−Pt(IV) dinuclear adducts which simply share a common Pt(IV) acceptor. In other words, the IT intermediate of the net two-electron transfer consists of two localized degenerate states, Fe(III)−Pt(III)−Fe(II) and Fe(II)−Pt(III)−Fe(III), rather than two nondegenerate, more delocalized states formed through strong electronic coupling. Furthermore, the virtually identical redox potentials, IR and Raman spectra, IT absorption bandwidths, and crystallographic Fe−Pt distances for the two molecules implies that the presence of a second iron moiety bridged to the acceptor Pt(IV) center has very little effect on the electronic or structural properties of the donor−acceptor interaction. Therefore, the trinuclear complex can be conveniently modeled as consisting of two degenerate back-to-back donor−acceptor dyads: D−A/A−D, which happen to share a common molecular orbital as the acceptor (Figure 1f).

The above conclusions are in contrast to those observed for a similar D−A−D trinuclear species, $[(NC-Ru^{II}(bpy)_2-CN-Ru^{III}(bpy)_2-NC-Ru^{II}(bpy)_2-CN]^{3+}$ (where bpy = 2,2′-bipyridine), which was previously reported by Scandola et al.[5e] These authors report the presence of two overlapping IT absorptions, which have similar energies. The presence of two IT bands has been interpretted as arising from a significant electronic coupling between the degenerate Ru(III)−Ru(II)−Ru(II) and Ru(II)−Ru(II)−Ru(III) excited states (Figure 1g). There are several important distinctions to be made between the two systems which might account for the observed differences in their electronic spectra and the degree of electronic coupling between remote metal centers. These include the larger redox asymmetry of the Fe(II)−Pt(IV)−Fe(II) complex, the differing degrees of π-back-bonding between the various metals and the ligand bridges, the higher energy of the Pt(III) IT excited state, and the different point groups of the two molecules.

Photochemistry. Irradiation of the IT absorption band of $[(NH_3)_5Pt^{IV}(\mu\text{-NC})Fe^{II}(CN)_5]$ at 488 nm led to a gradual decrease in the intensity of the IT band and the growth of a charge-transfer band at 303 nm. In a preliminary experiment, a 16 mM solution of the compound was irradiated until no further changes occurred in its electronic absorption spectrum. The UV/vis spectrum which resulted had a triad of peaks centered at 303 nm and a less intense peak at 416 nm. This spectrum very closely resembled that of the ferricyanide ion. Cyclic voltammetry of the photoproduct revealed a new redox event occurring with $E_{1/2}$ = 0.19 V vs SCE, identical to that observed for $K_3Fe(CN)_6$. Biasing the electrode potential at 0 V vs SCE led to a cathodic current, confirming the 3+ oxidation state of iron in the observed solution photoproduct. The quantum efficiency for loss of the dinuclear compound, as measured at 488 nm, was 0.014 at 293 K. The quantum efficiency for formation of the ferricyanide product (as measured by formation of the peak at 303 nm after correction for the absorption of the dinuclear compound at that wavelength) was 0.012 under identical conditions. Irradiated solutions at higher concentrations undergo a back-electron-transfer reaction over time when they are stored in the dark, partially re-forming a species which has a UV/vis spectrum similar to that of the original. A brownish-red solid photoproduct was also observed at very high concentrations. Infrared spectroscopy of this product revealed a broad ν(CN) stretch at ∼2060 cm^{-1} with a less intense shoulder at ∼2110 cm^{-1}, indicating the presence of both terminal and bridging Fe(II) cyanides. The identity of the solid photoproduct has not yet been confirmed. It is postulated that the product contains a polymeric $[Fe(II)-Pt(IV)]_n$ species formed by the back-reaction of ferricyanide with Pt(II) ammines at these higher concentrations.

Summary

To better understand the photophysics of the trinuclear mixed-valence compound, $[(NC)_5Fe^{II}(\mu\text{-CN})Pt^{IV}(NH_3)_4(\mu\text{-NC})Fe^{II}(CN)_5]^{4-}$, which has a degenerate one-electron excited state, the corresponding dinuclear $[(NH_3)_5Pt^{IV}(\mu\text{-NC})Fe^{II}(CN)_5]\cdot 6H_2O$ compound was synthesized and investigated. The electrochemistry and spectroscopy of these two compounds are extremely similar, implying that the initial one-electron photophysics of the former compound can be modeled as a single Fe(II) → Pt(IV) IT transition, which is relatively unaffected by the presence of a second Fe(II) center.

Acknowledgment. The authors acknowledge Dr. T. G. Spiro for the use of his resonance Raman equipment and Dr. Z. Soos for stimulating conversations about the theoretical aspects of this paper. J.V.L. and B.W.P. are grateful for the support of the Camille & Henry Dreyfus Foundation in the form of a faculty start-up grant. This work was also funded by the National Science Foundation under Grant CHE-9631380.

Supporting Information Available: Tables listing details of the crystal structure refinement information, the atomic coordinates and equivalent isotropic displacement parameters, all nonequivalent bond distances and bond angles, anisotropic displacement parameters, and hydrogen atomic coordinates and isotropic displacement parameters and figures depicting the unit cell and extended views along the crystallographic axes *a*, *b*, and *c*, showing the positions of the waters of hydration. This material is available free of charge via the Internet at http://pubs.acs.org.

IC981441A

(24) The parameter *r* can be less than the geometric donor−acceptor distance in molecules with a significant degree of delocalization. See, for instance: Karki, L.; Hupp, J. T. *J. Am. Chem. Soc.* **1997**, *119*, 4070.